$^{40}Ar/^{39}Ar$ geochronology of the Ocate volcanic field, north-central New Mexico

Brian W. Olmsted[1] and William C. McIntosh[2]
[1]Department of Earth and Environmental Science, New Mexico Institute of Mining and Technology, Socorro, NM 87801
[2]New Mexico Bureau of Geology and Mineral Resources, New Mexico Institute of Mining and Technology, Socorro, NM 87801

Abstract

Eighty-two $^{40}Ar/^{39}Ar$ analyses from 70 basaltic samples from the Ocate volcanic field reveal that the field erupted episodically in approximately 14 pulses between 8.2 and 0.8 Ma. In general, a north-to-south time progression of volcanism occurred during the evolution of the field. The two largest eruptive episodes, 5.13–4.35 and 3.36–2.85 Ma, produced approximately 32 and 40 vol. % (28 and 36 km^3) of the field (90 km^3 total), respectively. After, and possibly just before, the 5.13–4.35 Ma eruptions, a period of tectonic activity with extensive down-to-the-west faulting took place within the western part of the field. Following the 3.36–2.85 Ma eruptions, a period of decreased eruptive activity with small, localized eruptive centers ensued within the central and southern parts of the field. Minimum erosion rates calculated utilizing the inverted topography within the field generally decrease from 6 Ma to present.

Introduction

The Ocate volcanic field is located in north-central New Mexico within the transition zone between the Great Plains and Rocky Mountain physiographic provinces, just east of the Rio Grande rift (Figs. 1, 2). The field is one of several dominantly basaltic late Miocene-Pleistocene eruptive complexes that define the Jemez lineament in northern New Mexico (Fig. 1). Northeast of the Ocate field lies the Raton–Clayton volcanic field and to the northwest, within the Rio Grande rift, lies the Taos volcanic field. The Ocate field is bounded to the west by the southern Sangre de Cristo Mountains, to the east by the Canadian River, to the north by the Cimarron Range, and to the south by the Mora River. Volcanic rock compositions in the Ocate field range from alkali olivine basalt to dacite, with the predominant rock type being basaltic lavas erupted from shield volcanoes, composite cones, fissures, and cinder cones (Nielsen and Dungan 1985; O'Neill and Mehnert 1988).

Based on 16 K-Ar analyses, previous workers determined that eruptive activity within the Ocate field ranged from 8.3–0.8 Ma (O'Neill and Mehnert 1988). The field exhibits inverted topography where the oldest flows cap the highest mesas and younger flows cap lower mesas. Based on analysis of the physiographic evolution of the field, O'Neill (1988)

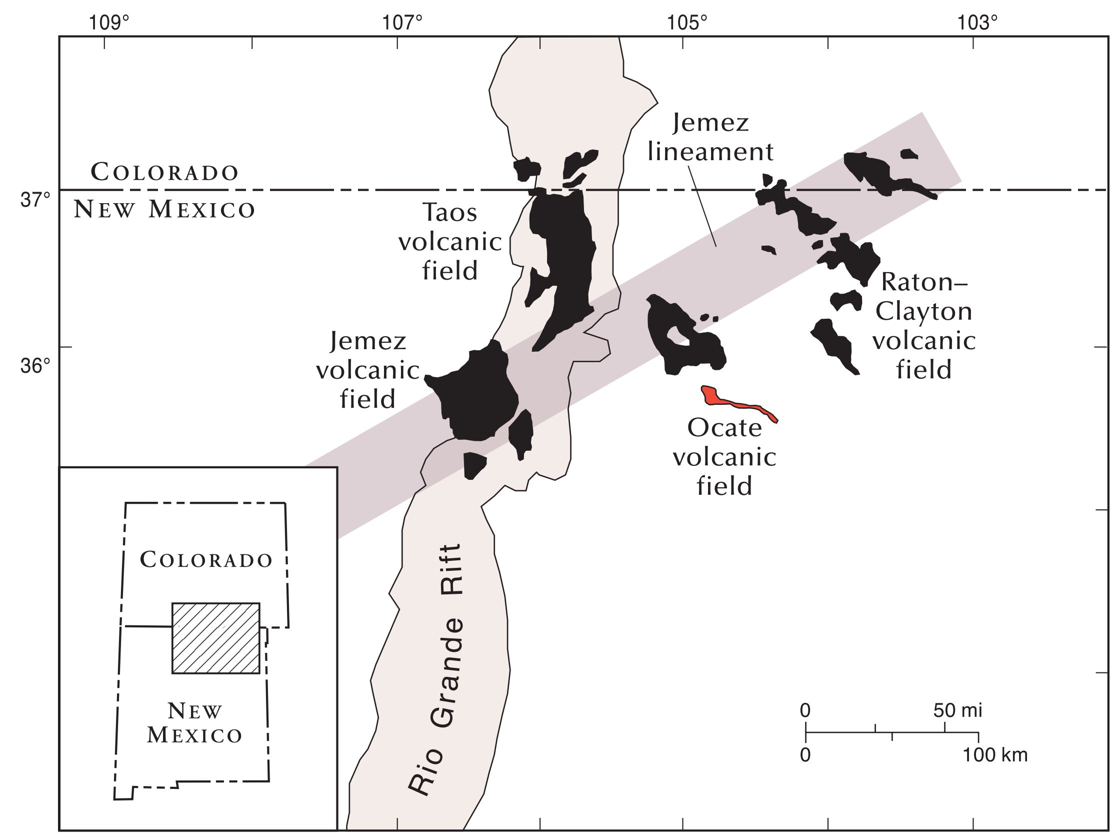

FIGURE 1—Late Cenozoic volcanic fields near the intersection of the Rio Grande rift and Jemez lineament in northern New Mexico and southern Colorado.

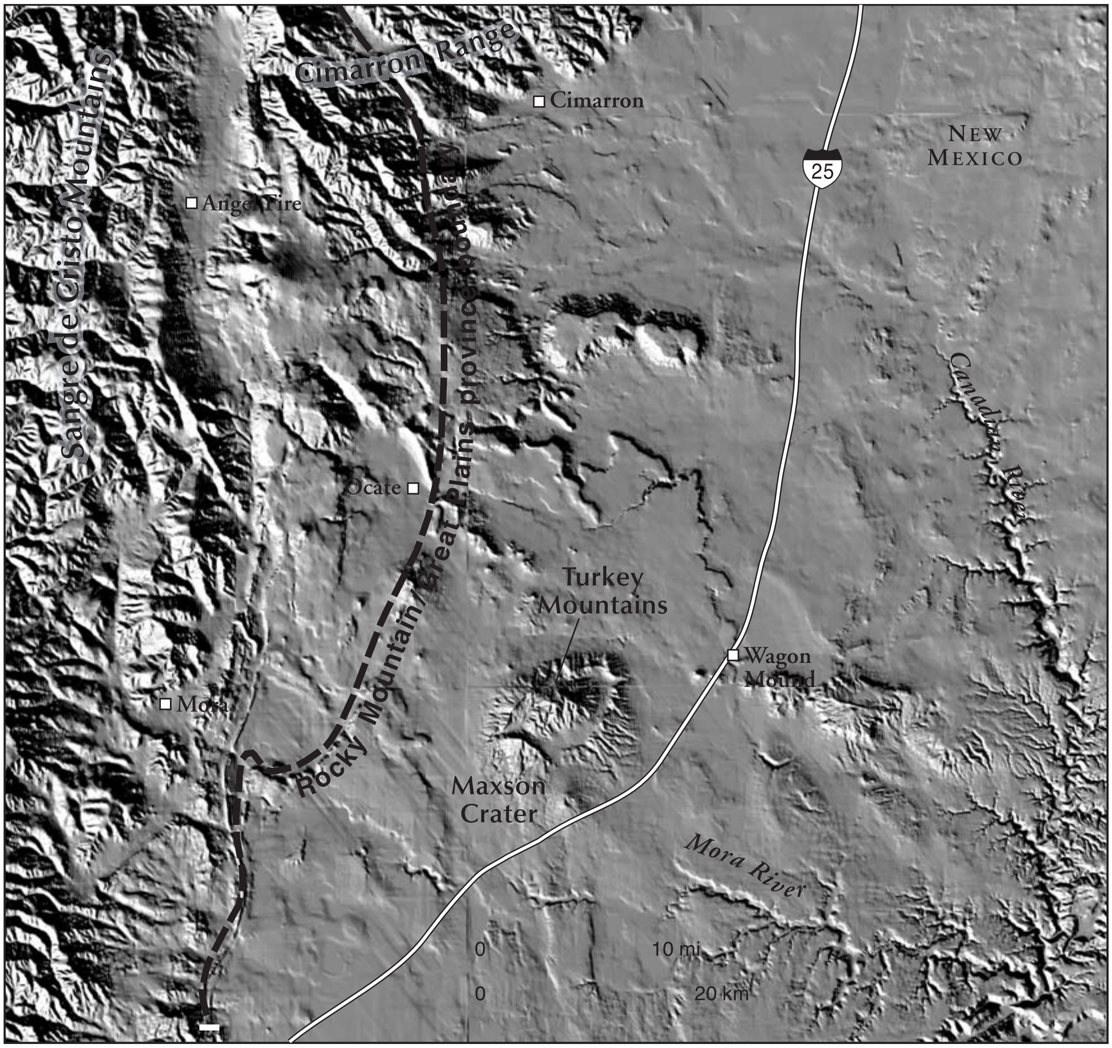

FIGURE 2—Shaded relief map of the Ocate volcanic field.

suggested that volcanism in the Ocate area was coeval with the epieorgenic rise of the Sangre de Cristo Mountains and the adjacent Great Plains.

The purpose of this study was to improve the precision, accuracy, and completeness of the eruptive chronology of the Ocate volcanic field. The $^{40}Ar/^{39}Ar$ dating technique was used because of its high precision and potential ability to detect and correct for extraneous ^{40}Ar, radiogenic ^{40}Ar loss and xenocrystic contamination (McDougall and Harrison 1999). The $^{40}Ar/^{39}Ar$ ages determined in this study are used to reconstruct the eruptive history, both spatially and temporally, and to constrain the landscape evolution of the Ocate field.

Methods and results

Field methods

Samples were collected from 83 locations throughout the field. Where possible, non-vesicular, well crystallized and non-weathered flow interior samples were collected. Sample locations were measured with a hand-held GPS unit. Seventy of the 83 total samples were selected for $^{40}Ar/^{39}Ar$ analysis.

Approximately 10% of the field could not be sampled because permission was denied to access the privately owned Ojo Feliz Ranch located within the central part of the field. This area includes what is probably the youngest eruption in the Ocate field, the Cerro del Oro lava dated by K-Ar at 0.81 ± 0.14 Ma (O'Neill and Mehnert 1988). This K-Ar age determination is combined with the new $^{40}Ar/^{39}Ar$ data in reconstructions of the eruptive history in this paper.

$^{40}Ar/^{39}Ar$ analytical methods

Samples were crushed and sieved to 20–48 mesh (300–850 µm), ultrasonically cleaned with dilute HCl and then ultrasonically washed with deionized water. Using a binocular microscope, care was taken to remove all visible phenocryst/xenocryst phases from the groundmass concentrates to increase the percentage of potassium within the final bulk sample and to decrease the potential affects of extraneous argon (McDougall and Harrison 1999).

Samples were irradiated in several batches for durations of 1–7 hrs in either the D-3 position at the Nuclear Science Center reactor at Texas A & M University, or the L-6 position at the Ford Reactor at the University of Michigan. Fish Canyon Tuff sanidine with an assigned age of 27.84 Ma (Deino and Potts 1990; equivalent to Mmhb-1 at 520.4 Ma) was used as a flux monitor.

Samples were analyzed at the New Mexico Geochronological Research Laboratory (NMGRL) at New Mexico Institute of Mining and Technology. All seventy were step-heated in a standard double-vacuum molybdenum resistance furnace and six samples were also step-heated using a defocused CO_2 laser beam. Details of sample preparation, irradiation, and analyses are listed in the footnotes to Table 1. Additional information is available in Olmstead (2000).

TABLE 1—Summary of $^{40}Ar/^{39}Ar$ results from Ocate volcanic field.

Sample	Geographic location	Sample type	Longitude	Latitude	Elevation (m)	n[1]	^{39}Ar (%)[2]	Age (Ma) ± error (2σ)
OCA-001	Maxson Crater	Flow surface	104.8575	35.8783	2,300	3	36.7	1.58 ± 0.16
OCA-002	Guadalupita Canyon	Flow interior	105.2364	36.2419	2,890	3	65.3	4.45 ± 0.02
OCA-003	La Mesa	Flow interior	105.1557	36.0417	2,590	3	65.8	4.45 ± 0.05
OCA-004-01	Maxson Crater	Flow interior	104.3864	35.7284	1,600	1	17.7	1.56 ± 0.06
OCA-004-02	Maxson Crater	Flow interior	104.3864	35.7284	1,600	7	61.8	1.64 ± 0.05
OCA-005	Maxson Crater	Flow surface	104.3864	35.7294	1,610	3	36.2	1.59 ± 0.15
OCA-006	Maxson Crater	Flow interior	104.3869	35.7390	1,620	5	56.1	1.57 ± 0.06
OCA-007	Maxson Crater	Flow interior	104.3867	35.7385	1,630	5	66.4	1.54 ± 0.07
PW-OCA-007[3]	Maxson Crater	-	104.8936	35.8615	2,280	4	67.9	1.56 ± 0.02
OCA-008-01	Charette Mesa	Flow interior	104.7138	36.0044	2,160	2	48.1	2.98 ± 0.05
OCA-008-02	Charette Mesa	Flow interior	104.7138	36.0044	2,160	5	69.6	3.01 ± 0.04
OCA-009	Charette Mesa	Flow interior	104.7126	36.0142	2,170	3	47.9	2.90 ± 0.04
OCA-010	Ocate Creek area	Flow interior	105.1147	36.2376	2,770	2	55.1	2.51 ± 0.09
OCA-011	Laguna Salada Mesa	Flow interior	105.1831	36.2921	3,270	3	62.9	5.67 ± 0.03
OCA-012	Cerro Pelon	Flow interior	105.0538	36.1617	2,510	4	75.7	2.98 ± 0.03
OCA-013	Cerro Vista Mesa	Flow interior	105.4483	36.1349	3,380	7	81.3	5.65 ± 0.03
OCA-014	Las Mesas del Conjelon	Flow interior	104.6466	35.9886	2,300	3	55.0	6.03 ± 0.03
OCA-016	Charette Mesa	Flow interior	104.8155	36.2085	2,300	7	80.5	3.20 ± 0.04
OCA-019	Apache Mesa	Flow interior	104.9056	36.1846	2,510	4	69.2	4.59 ± 0.02
OCA-020	Cerrito Pelon	Flow interior	104.9100	36.1875	2,460	10	87.4	2.28 ± 0.03
OCA-022	Cerro Negro area	Vent	104.8855	36.1189	2,500	6	69.3	2.36 ± 0.14
OCA-023	Cerro Negro area	Vent	104.8707	36.1148	2,470	5	58.9	1.80 ± 0.02
OCA-024	Cooks Peak	Flow interior	105.0438	36.2414	3,010	6	79.7	4.40 ± 0.03
OCA-025	Gallinas Mesa	Flow interior	105.0544	36.2244	2,990	5	60.9	7.04 ± 0.04
OCA-026	Apache Mesa (West)	Flow interior	104.9989	36.2260	2,770	2	38.0	5.71 ± 0.04
OCA-027	Apache Mesa (West)	Flow interior	105.0018	36.2355	2,930	4	57.2	5.73 ± 0.02
OCA-028	Rivera Mesas	Flow interior	105.0018	36.2573	2,790	7	81.0	4.37 ± 0.02
OCA-029	El Cerro Colorado	Vent	105.2763	36.0646	2,610	5	62.3	4.44 ± 0.03
OCA-030	Palo Flechado Mesa	Flow interior	105.3736	36.4071	3,380	4	55.2	20.89 ± 0.08
OCA-030L1[4]	Palo Flechado Mesa	Flow interior	105.3736	36.4071	3,380	4	79.0	21.14 ± 0.14
OCA-030L2[4]	Palo Flechado Mesa	Flow interior	105.3736	36.4071	3,380	2	64.2	21.11 ± 0.10
OCA-031	Maxson Crater	Vent	104.8914	35.9016	2,560	3	26.7	1.57 ± 0.04
OCA-032	Black Mesa	Flow interior	105.0849	35.9734	2,610	5	79.7	4.59 ± 0.03
OCA-033	Black Mesa area	Flow interior	105.0800	35.9746	2,560	5	55.7	2.31 ± 0.05
OCA-034	Cerro Pelon	Flow interior	105.0388	35.9606	2,410	6	62.1	2.27 ± 0.03
OCA-035	El Cerro Colorado	Flow interior	105.2356	36.0451	2,770	4	52.5	4.43 ± 0.03
OCA-036	Urraca Mesa	Flow interior	104.9941	36.4127	2,840	5	36.1	4.51 ± 0.06
OCA-036L	Urraca Mesa	Flow interior	104.9941	36.4127	2,840	6	89.8	4.50 ± 0.08
OCA-037	Rayado Mesa	Flow interior	104.9038	36.2936	2,540	7	81.8	4.46 ± 0.04
OCA-038	Rivera Mesas area	Flow interior	104.9254	36.2646	2,540	7	90.4	4.42 ± 0.02
OCA-039	Rivera Mesas area	Flow interior	104.9184	36.2499	2,440	4	44.8	3.47 ± 0.05
OCA-040	Rivera Mesas area	Flow interior	104.9221	36.2681	2,460	4	44.4	3.53 ± 0.04
OCA-041	Rivera Mesas area	Flow interior	104.9239	36.2748	2,500	5	54.4	3.51 ± 0.02
OCA-042	Ortega Mesa	Flow interior	104.9282	36.2765	2,540	5	47.6	4.42 ± 0.09
OCA-043	Le Febres Mesa	Flow interior	105.1039	36.1724	2,640	4	54.1	3.01 ± 0.04
OCA-044	Le Febres Mesa	Flow interior	105.0781	36.2075	2,610	5	66.4	3.01 ± 0.03
OCA-045	Le Febres Mesa	Flow interior	105.1355	36.1888	3,010	5	64.7	3.05 ± 0.04
OCA-046	La Mesa	Vent	105.2123	36.2393	3,440	4	65.7	4.64 ± 0.07
OCA-047	Ocate Mesa	Flow interior	105.2035	36.2672	3,430	3	51.9	8.16 ± 0.03
OCA-048	Guadalupita Canyon	Flow interior	105.2298	36.1867	2,730	6	85.5	4.48 ± 0.02
OCA-051	Agua Fria Peak	Vent	105.2066	36.3587	3,850	6	71.3	4.98 ± 0.04
OCA-052	Agua Fria area	Flow interior	105.2443	36.3725	3,580	5	51.3	4.99 ± 0.03
OCA-053	Moreno Valley	Flow interior	105.2617	36.4159	3,020	4	48.4	6.57 ± 0.04
OCA-054	La Grulla Ridge	Flow interior	105.1406	36.3335	3,450	4	62.8	8.17 ± 0.04
OCA-055	Le Febres Mesa	Flow interior	105.1591	36.1511	2,920	8	81.8	3.00 ± 0.03
OCA-057	Charette Mesa area	Flow interior	104.7035	36.0450	2,170	7	76.6	2.20 ± 0.02
OCA-059	Las Mesas del Conjelon	Flow interior	104.7474	36.0092	2,370	7	79.6	6.03 ± 0.02
OCA-061	Maxson Crater area	Flow interior	104.7216	35.9331	2,170	6	64.0	2.28 ± 0.03
OCA-062	Laguna Salada Mesa	Flow interior	105.1395	36.2733	32,40	8	86.1	6.43 ± 0.03
OCA-063	Cerro Negro	Vent	104.9331	36.1113	26,20	4	73.1	1.97 ± 0.03
OCA-064	Encinosa Mesa	Flow interior	104.9413	36.1169	2,620	6	73.0	6.40 ± 0.08
OCA-066	Fowler Mesa	Flow surface	105.0564	36.3958	3,200	4	32.5	4.47 ± 0.06
OCA-067	Fowler Mesa	Flow surface	105.0564	36.3958	3,200	5	43.4	4.48 ± 0.03
OCA-068	Las Mesas del Conjelon	Flow interior	104.6959	36.0005	2,340	5	81.7	6.07 ± 0.02
OCA-069	Cerrito Pelon	Flow interior	105.0114	36.1943	2,550	6	75.1	2.35 ± 0.02
OCA-070	Ortega Mesa	Flow interior	105.0564	36.3079	3,020	6	57.3	4.68 ± 0.03
OCA-071	White Peak	Vent	105.0197	36.2980	3,060	4	45.9	3.53 ± 0.08
OCA-073-01	Rivera Mesa	Flow surface	105.0226	36.2443	2,780	3	20.5	3.50 ± 0.06
OCA-073-02	Rivera Mesa	Flow surface	105.0226	36.2443	2,780	5	26.0	3.52 ± 0.07
OCA-073L[4]	Rivera Mesa	Flow surface	105.0226	36.2443	2,780	5	73.6	3.54 ± 0.12
OCA-075	Encinosa Mesa	Flow interior	104.9714	36.1209	2,700	6	76.4	6.39 ± 0.06
OCA-077	Cerro Negro area	Flow interior	104.9526	36.1159	2,650	4	57.7	1.96 ± 0.03
OCA-077L[4]	Cerro Negro area	Flow interior	104.9526	36.1159	2,650	5	91.9	1.97 ± 0.04

TABLE 1—continued.

Sample	Geographic location	Sample type	Longitude	Latitude	Elevation (m)	n[1]	^{39}Ar (%)[2]	Age (Ma) ± error (2σ)
OCA-078	Las Mesas Del Conjelon	Flow interior	104.7316	36.0082	2,370	4	69.5	6.02 ± 0.04
OCA-079	Cerro Pelon	Flow surface	105.1037	36.0408	2,600	3	48.0	2.18 ± 0.04
OCA-079L1[4]	Cerro Pelon	Flow surface	105.1037	36.0408	2,600	3	90.0	2.13 ± 0.05
OCA-079L2[4]	Cerro Pelon	Flow surface	105.1037	36.0408	2,600	5	88.7	2.11 ± 0.02
OCA-080	Cerro Montoso area	Flow interior	105.1435	36.0754	2,670	3	36.4	3.31 ± 0.05
OCA-081	Laguna Salada Mesa	Flow interior	105.1462	36.2819	3,290	4	48.6	5.09 ± 0.04
OCA-082	Agua Fria area	Flow interior	105.2038	36.2851	3,260	7	84.4	4.48 ± 0.03
Cerro Mont.	Cerro Montoso	Vent	105.1813	36.1335	31,60	5	86.5	3.07 ± 0.10

[1]Number of heating steps used in the eruption age calculation

[2]Total percent ^{39}Ar released of heating steps used in the eruption age calculation

[3] Sample collected by Paul Wisniewski.

[4]Laser-step-heating anlysis, all other analyses heated by resistance furnace

Sample preparation and irradiation:

Groundmass concentrates prepared by coarse crushing and hand-picking fragments free of visible phenocrysts.

Samples irradiated in machined Al discs between 1 and 7 hrs in either the D-3 position, Nuclear Science Center, College Station, TX, or the L-6 position, Ford Reactor, University of Michigan.

Neutron flux monitor Fish Canyon Tuff sanidine (FC-1). Assigned age = 27.84 Ma (Deino and Potts 1990) equivalent to Mmhb-1 at 520.4 Ma (Samson and Alexander 1987).

Instrumentation:

Mass Analyzer Products 215-50 mass spectrometer on line with automated all-metal extraction system.

Samples step-heated in either a Mo double-vacuum resistance furnace or a defocused CO_2 laser beam. Heating duration per step of 7 min for furnace and 13 min for laser.

Reactive gases removed by reaction with 3 SAES GP-50 getters, 2 operated at ~450°C and 1 at 20°C. Gas also exposed to a W filament operated at ~2,000°C.

Analytical parameters:

Electron multiplier sensitivity averaged 2 x10^{-16} moles/pA for the furnace and 1 x10^{-16} moles/pA for the CO_2 laser.

Total system blank and background for the furnace averaged 640, 4.8, 0.7 , 2.0, and 2.6 x 10^{-18} moles at masses 40, 39, 38, 37, and 36, respectively for temperatures <1,300°C.

Total system blank and background for the laser averaged 330, 4.2, 0.6 , 2.1, and 2.4 x 10^{-18} moles at masses 40, 39, 38, 37, and 36, respectively for temperatures <1,300°C.

J-factors determined to a precision of ± 0.1% by CO_2 laser-fusion of 4 single crystals from each of 6 radial positions around the irradiation tray.

Correction factors for interfering nuclear reactions were determined using K-glass and CaF_2 and are as follows: (^{40}Ar/^{39}Ar)K = 0.00020 ± 0.0003; (^{36}Ar/^{37}Ar)Ca = 0.00026 ± 0.00002; and (^{39}Ar/^{37}Ar)Ca = 0.00070 ± 0.00005.

Age calculations:

Eruption ages calculated for the indicated steps by weighting each step by the inverse of the variance.

Eruption age errors calculated using the method of Sampson and Alexander (1987).

Decay constants and isotopic abundances after Steiger and Jäger (1977).

All errors reported at ± 2σ, unless otherwise noted.

Age assignment methods

^{40}Ar/^{39}Ar analytical data and age spectra are presented in Appendices 1 and 2. Consistent apparent ages for consecutive steps within the mid-temperature range were chosen to represent the eruption age of each sample. Uncertainties in eruption ages are reported at the 2σ confidence level and include errors in J-value, system blank, isotope peak-height regression, mass discrimination, and interfering reaction constants. Eruption ages are weighted by the inverse of the variance for the steps selected and uncertainties are calculated using the method of Samson and Alexander (1987). See Olmsted (2000) for full description of the interpretation of ^{40}Ar/^{39}Ar data.

Method of eruption volume calculation

Volumes of mapped flow units were estimated as a function of their adjusted surface area as detailed in Olmstead (2000) and Appendix 3. Present-day surface areas were first determined from digitized maps. These measured areas were then adjusted to account for estimates of buried or eroded portions of flows and for estimated average flow thickness. Lastly, approximate volumes were calculated by expressing the adjusted area of each unit as a fraction of cumlative area, then multiplying these by 90 km^3, the total volume of the Ocate volcanic field estimated by Neilsen and Dungan (1985). Calculated volumes are summarized in the inset table in Figure 5.

Results

Table 1 summarizes the argon results for each sample as well as listing their locations and the sample type (i.e., samples collected from the surface of a flow, interior of a flow, or proximal to the eruptive vent). Figure 3 displays the results of replicate analyses and analyses of multiple samples from a given flow unit. In general, there is excellent agreement of most replicate and multiple sample analyses, as shown by mean square of weighted deviates (MSWD) values indicating that observed variation can be attributed to analytical error (Mahon 1996). Two of the replicate analysis and two of the multiple sample analysis data sets (Fig. 3) show small but significant age differences and higher MSWD values indicating age differences slightly larger than can be readily attributed to analytical error, reflecting either underestimation of analytical error, or influence of sample problems such as alteration or ^{39}Ar recoil.

Figure 4 is a graph of previously published K-Ar ages versus the new ^{40}Ar/^{39}Ar ages for pairs of samples from the same flow unit. The results show that the new ^{40}Ar/^{39}Ar eruption ages have analytical errors less than half of those obtained with the K-Ar method. Eleven of the 13 flow units dated by both the K-Ar and ^{40}Ar/^{39}Ar methods are within analytical error of each other, whereas 2 of the 13 analyses are not.

Interpretation and discussion

Precision and accuracy of $^{40}Ar/^{39}Ar$ results

The results of the replicate analyses (Fig. 3) show that the eruption ages for five out of the seven samples studied are reproducible and yield individual eruption ages for each sample that are within error of each other. One out of the three analyses for both OCA-030 and OCA-079 are not within error of the two other analyses at the 95% confidence level. Because of this, for both of these samples the MSWD value is greater than what can be attributed to analytical error (Mahon 1996). This may be due to underestimation of the analytical uncertainty for one or more of the analyses.

The results of analyses of multiple samples from a given flow unit (Fig. 3) show that six of the eight flow units display single statistical populations with analytically acceptable MSWD values , whereas two of the eight flow units (Cerrito Pelon and Las Mesas del Conjelon) display MSWD values that are greater than what can be attributed to only analytical uncertainty. The high MSWD values for the Cerrito Pelon and Las Mesas del Conjelon analyses may be due to an underestimate of the analytical uncertainty for one or more of the analyses, the presence of a statistical outlier at the 95% confidence level, or the occurrence of two or more eruptive events closely spaced in time.

Comparison of K-Ar ages and $^{40}Ar/^{39}Ar$ ages (Fig. 4) along with the agreement of total gas and eruption ages for individual $^{40}Ar/^{39}Ar$ analyses (Olmsted 2000) suggests excess ^{40}Ar and radiogenic ^{40}Ar loss are not significant factors affecting the results. In addition, it is clear that the higher precision of the $^{40}Ar/^{39}Ar$ technique is superior to K-Ar for resolving closely spaced volcanic events in the Ocate volcanic field, differing in age by as little as 100,000 yrs (Fig. 4).

Based on the K-Ar results determined by O'Neill and Mehnert (1988), seven pulses of eruptive activity can be discerned. Based on the new $^{40}Ar/^{39}Ar$ results, these broad pulses of eruptive activity initially determined by O'Neill and Mehnert (1988) are now more precisely defined, resulting in an increased understanding of the overall eruptive history of the field. In addition, due to the greater number of samples collected and analyzed for this study, several new pulses of activity as well as distinct hiatuses in eruptive activity are apparent (Figs. 4, 5).

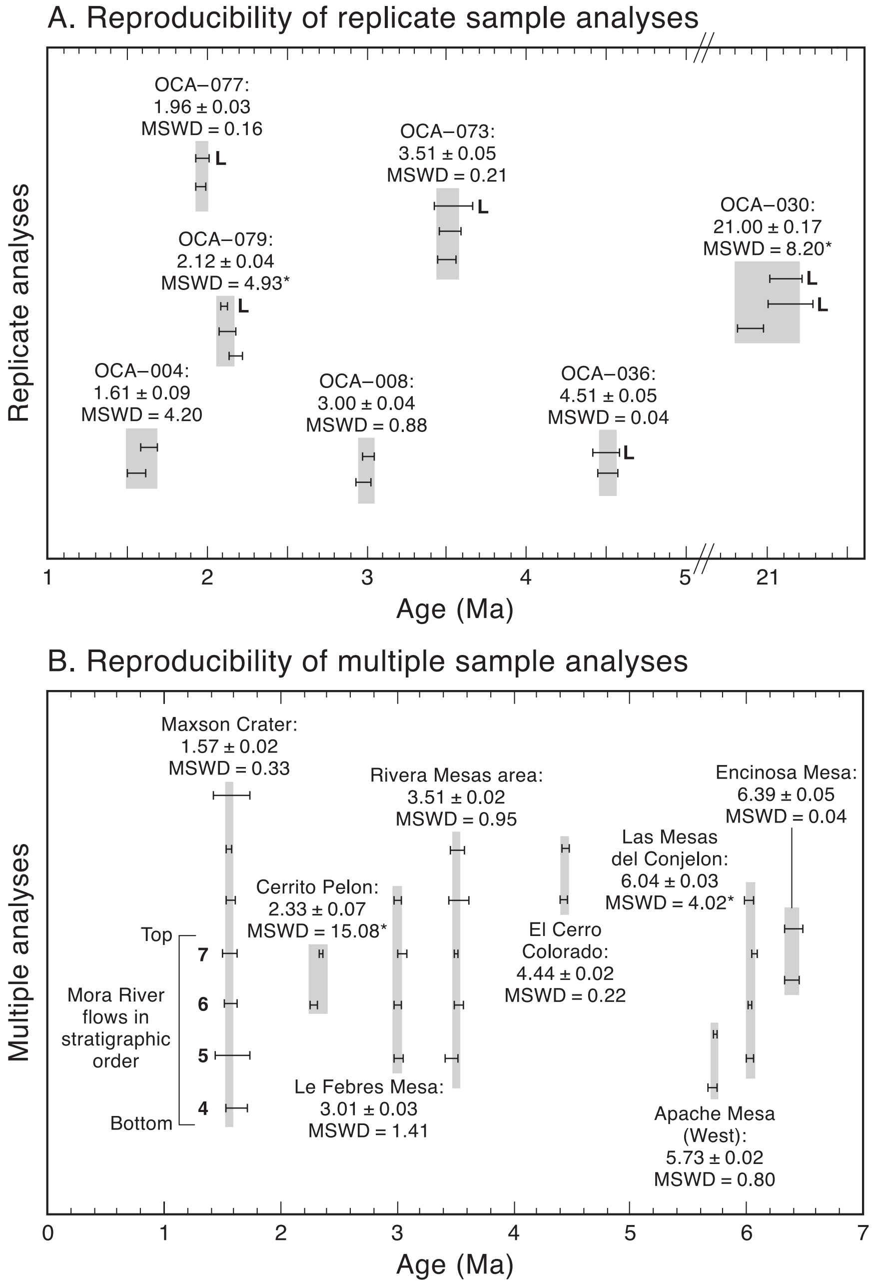

FIGURE 3—Reproducibility of $^{40}Ar/^{39}Ar$ age determinations. **A**. Replicate analyses of individual samples, with weighted mean and MSWD. **B**. Multiple samples from individual mapped units, with weighted mean and MSWD. Samples of the sequence of flows erupted from Maxson Crater and exposed along the Mora River are shown in stratigraphic order and identified by sample number. Sample OCA-004 represents weighted mean of two replicate analyses. L denotes laser-heated analyses, * denotes MSWD values greater expected from analytical error.

Spatial distribution of ages

Figure 5 displays the spatial distribution of ages along with the estimated eruption volumes for each flow unit. Except for Las Mesas del Conjelon, all eruptive centers greater than 3.5 Ma are within the northern and central parts of the field. A large percentage of these are focused in the northern part of the field around Agua Fria Peak. Eruptive centers less than 3.4 Ma occur within the central and southern part of the field. A basalt flow initially mapped as part of the Ocate volcanic field (O'Neill and Mehnert 1988) in the northwestern part of the field is dated at 20.89 ± 0.08 Ma (OCA-030). Based on the eruptive age, this flow is interpreted to be part of the Latir volcanic field (cf. Lipman et al. 1986).

Maxson Crater

Numerous remnants of individual flows originating from Maxson Crater are exposed along the base of the Mora River valley. At the confluence of the Mora and Canadian rivers

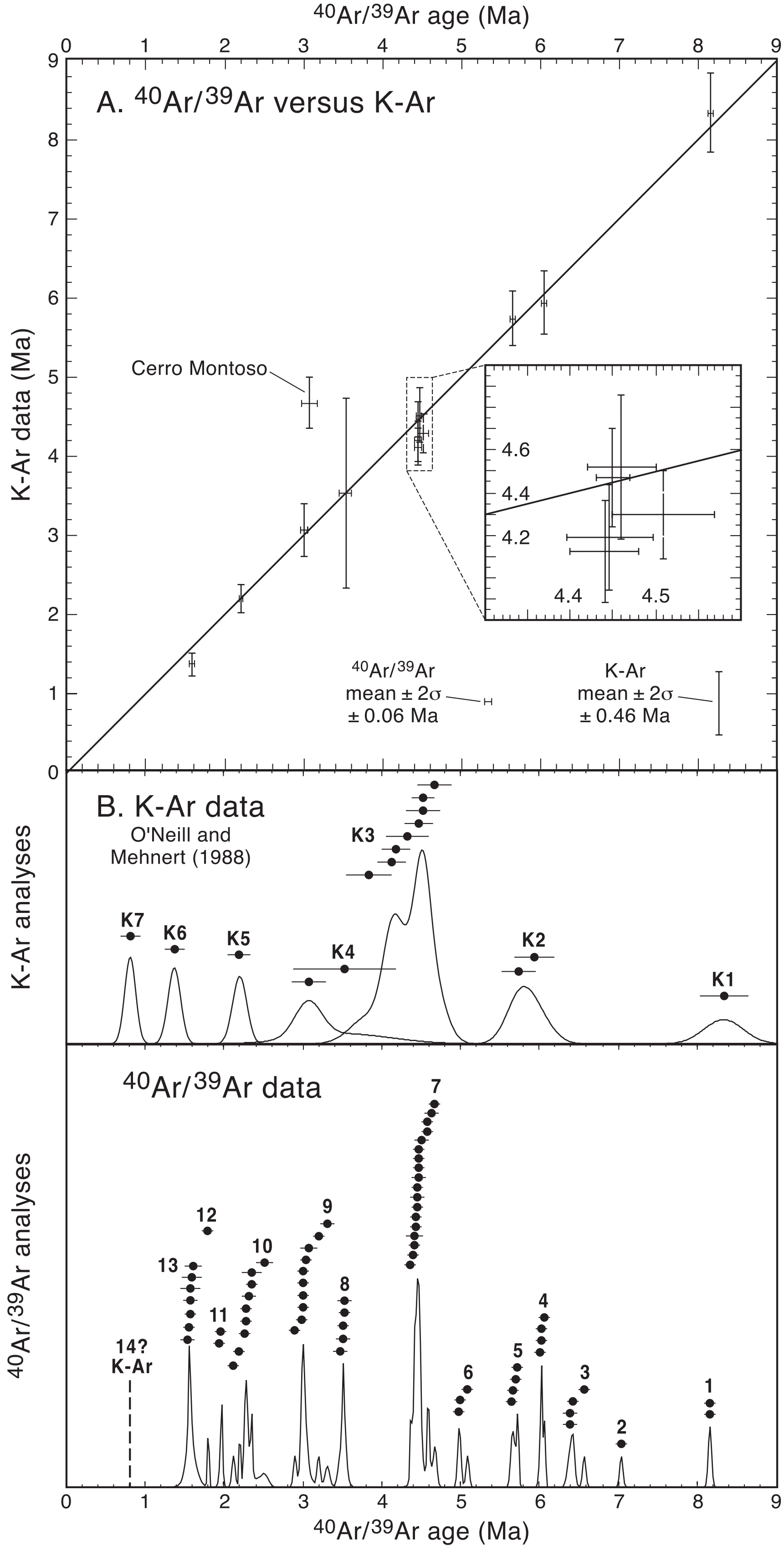

FIGURE 4—Comparison of previously published K-Ar dates from O'Neill and Mehnert (1988) with $^{40}Ar/^{39}Ar$ age determinations from this study. **A**. Comparative K-Ar and $^{40}Ar/^{39}Ar$ data for pairs of samples from various flow units, with ± 2σ error bars and a one-to-one reference line. **B**: Probability distribution plots of K-Ar and $^{40}Ar/^{39}Ar$ data. The $^{40}Ar/^{39}Ar$ data reveal narrower and more numerous eruptive pulses.

four of these flows were sampled in stratigraphic order so that the eruptive history could be assessed. The ages of all four samples agree within analytical error (Fig. 3). Furthermore, the ages obtained from samples collected proximal to the vent (OCA-001, PW-OCA-007, and OCA-031) also agree within analytical error of the samples collected in stratigraphic order (Table 1; Fig. 5). Therefore, it is concluded that the eruption of Maxson Crater occurred during a single pulse of activity at 1.57 ± 0.02 Ma.

Minimum erosion rates

Using the elevations of topographically inverted flows, minimum erosion rates can be quantified within parts of the field that have not experienced faulting since flow emplacement (Fig. 6 and Appendix 4). Erosion rates are calculated by dividing the elevation difference between the estimated bottom of a mesa and the adjacent valley floor by the age of the flow. The elevations were estimated from 7.5 min topographic maps with 20 ft contour intervals. Valley bottom elevations were chosen as the lowest point within the valley adjacent to where the mesa elevation was determined. In addition, in areas where two or more flow-capped mesas exist next to each other, erosion rates during intervals of time were quantified by dividing the elevation difference between the estimated flow-bottoms on two mesas by their age difference. Errors associated with the $^{40}Ar/^{39}Ar$ eruption ages were not incorporated in the erosion rate calculations. Several ages and elevations exist for Charette Mesa, therefore, the elevation and ages for samples closest to the area of interest were used in the calculation. The mean of the eruption ages for samples OCA-008 and OCA-009 were used for the age of Charette Mesa in the Las Mesas del Conjelon area.

Comparing changes in erosion rates with time can only be determined in localized areas due to the location-specific nature of calculated erosion rates. For example, comparison of the 80 m/Ma found at the Maxson Crater flows near the confluence of the Canadian and Mora rivers with the 8 m/Ma calculated near a small flow (2.28 Ma) between Las Mesas del Conjelon and Maxson Crater does not indicate an increase in erosion rate with time since 2.28 Ma. This is because the Maxson Crater flows represent a special localized case of erosion in a confined valley, geomorphically disturbed by being filled with lava. In contrast, the 8 m/Ma represents an area not greatly influenced by

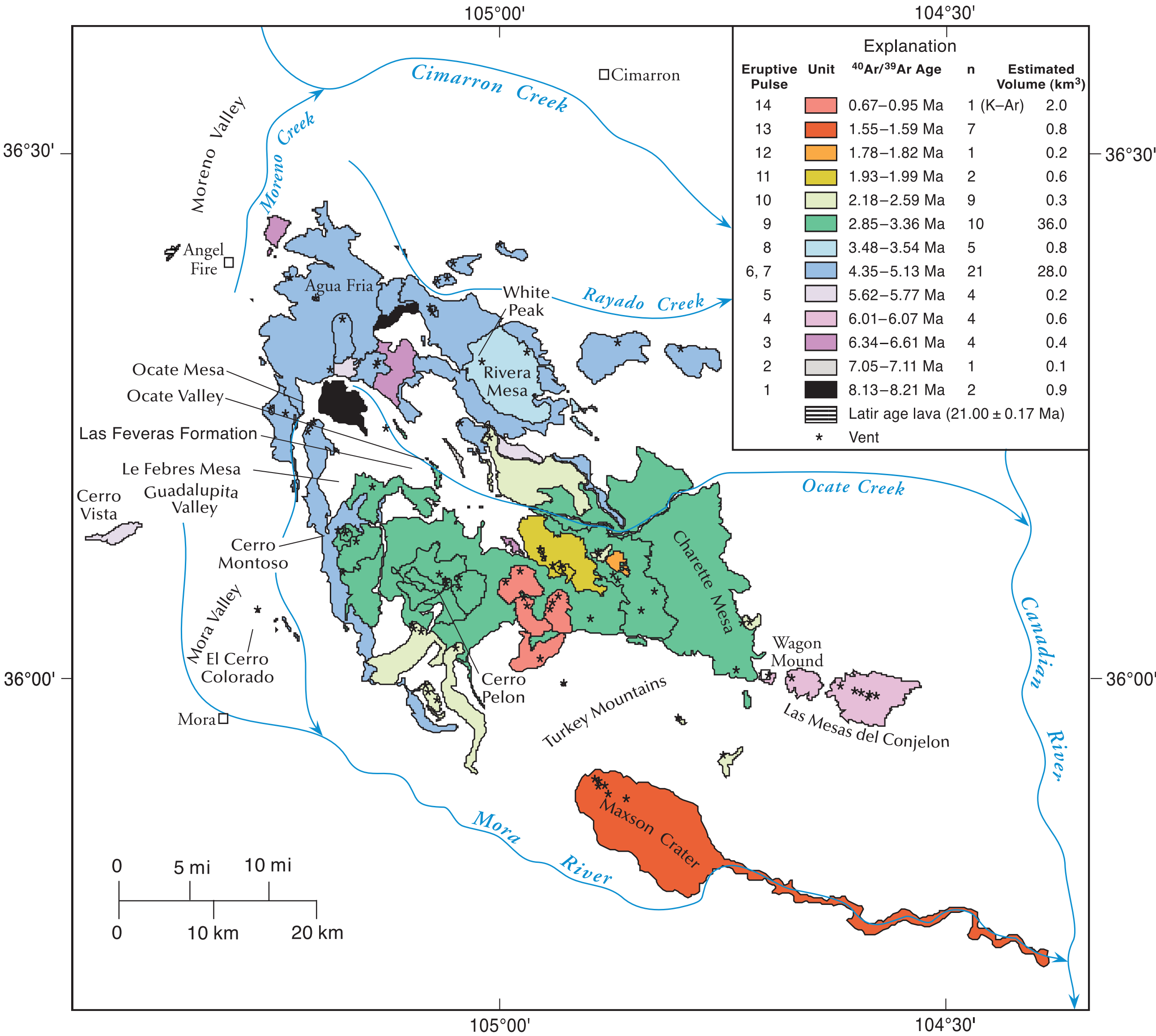

FIGURE 5—Map showing distribution of $^{40}Ar/^{39}Ar$ dated units in the Ocate volcanic field, modified from O'Neill and Mehnert (1988). Rivers and creeks are approximately located. Explanation indicates range of $^{40}Ar/^{39}Ar$ ages and estimated volumes for each eruptive pulse. **n** is the number of dated samples from each eruptive pulse.

the Mora river. By comparing calculated erosion rates from within areas that have experienced a common erosion history, more meaningful assessment of changing erosion rates through time can be made.

Multiple erosion rates suitable for assessment of temporal rate changes were calculated in three areas (northern, eastern, and southern) all located within the Great Plains physiographic province where individual lava flows rest on Cretaceous sedimentary rocks (Fig. 6). The northern area is located in the northwestern part of the volcanic field. It is a large horseshoe-shaped valley approximately 8 km north-south by 18 km east-west, which drains to the east. The eastern area is located within the east-central part of the volcanic field. It is located on the northern side of the eastern end of a shallow-sloping east-west topographic divide that extends to Cerro Pelon and further east to Cerro Montoso. The southern area is located in the south-central part of the volcanic field. The two lava-capped mesas sampled within this area rest above a gently-sloping plain that drains to the southeast.

Within the three areas where erosion rate changes were evaluated, the data indicate that erosion rates have decreased with time (Fig. 6). In addition, the actual values of the erosion rates for a given time period differ greatly between the different areas studied; this is inferred to be due to differences in erosional processes unique to each of the areas. The erosion rates calculated here are in the range of those found in a similar study done in the Raton–Clayton field (Stroud 1997). However, the increase in erosion rates from 8 Ma to present that Stroud (1997) found in the northeastern part of the Raton–Clayton field is not seen in the Ocate field. The seemingly contradictory results of the two studies may in part be due to the locations within the respective volcanic fields that the erosion rates were calculated. In the Raton-Clayton field the increase in erosion rates from 8 Ma to present is seen in the northwestern part of the field near the headwaters of the major drainages. In contrast, in the Ocate field the apparent decrease in erosion rates from 6 Ma to present is seen in the south, southeast, and northeast parts of the field, well away from the headwaters of the major drainages. Therefore, it is possible that in the Raton– Clayton field the increase in erosion rates from 8 Ma to present may reflect headward erosion. In the Ocate field, the apparent decrease in erosion rates with time may

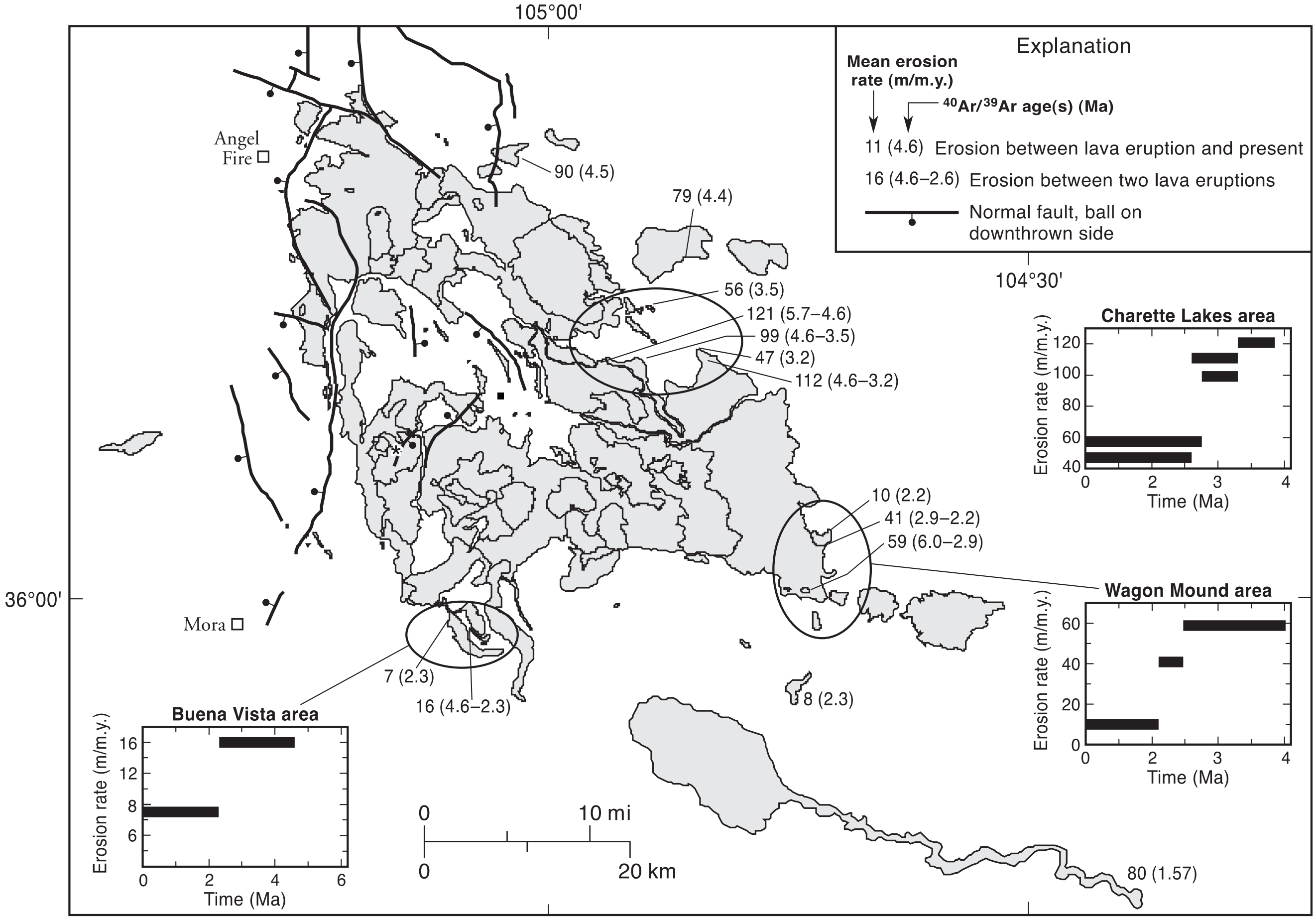

FIGURE 6—Map summarizing mean erosion rate calculations for the Ocate field. Inset graphs summarize results from three areas where changes in erosion rate through time were determined. At all three localities, mean erosion rates decreased between early (6–4 Ma) and late (3–0 Ma) Ocate volcanic field activity.

reflect decreased tectonic activity after 2–3 Ma or stabilization of base level on the major streams, perhaps by magmatic uplift of the Jemez lineament across the course of the Canadian river as suggested by Pazzaglia et al. (1999). In addition, the overall decrease in eruptive activity after the two volumetrically major eruptive episodes (5.13–4.35 and 3.36–2.85 Ma) directly corresponds with the decrease in erosion rates calculated within the field (Figs. 6, 7).

Vent locations and alignments

Figure 8 shows the spatial distribution of vent locations and the alignment of multiple vents for individual flow units. There appears to be a major structural control governing the alignment of vents. The Ocate volcanic field crosses the boundary between the southern Great Plains and Rio Grande rift paleostress provinces (Aldrich et al. 1986). The least principal horizontal stress in the southern Great Plains province has been oriented north-northeast-south-southwest to north-south since at least 28 Ma (Aldrich et al. 1986). The west-northwest vent alignments in the eastern Ocate field (Fig. 8) fit the southern Great Plains province whereas the vent alignments in the central and western Ocate field are more variable, perhaps reflecting the transition between the two paleostress provinces.

Flow directions

Figure 8 displays the flow directions based on the topography and vent location of the flow units. Except for the Cerro Vista flow, all flows were erupted onto a southeast sloping surface. Localized exceptions in flow directions are caused by topographic highs associated with the formation of volcanic edifices (e.g., Cerro Pelon and Agua Fria). The anticlines within the field appear to have been prominent topographic highs since the inception of volcanism. Evidence for this is seen by the lack of remnant flows on top of anticlines and flow directions deflected around the anticlines.

Timing of tectonic and geomorphic events

Onset of late Cenozoic faulting in the western part of the field appears to have occurred after the widespread 5.13–4.35 Ma eruptive pulse. Evidence for fault offset is seen in the El Cerro Colorado flow dated at 4.44 ± 0.04 Ma and in the Agua Fria flows dated at 4.48 ± 0.03 Ma (Fig. 8). Offsets at these two locations are approximately 275 and 183 m, respectively. Thus, minimum fault offset rates along this prominent fault at the El Cerro Colorado and Agua Fria sites are 62 and 41 m/Ma, respectively. Evidence along the southern part of this fault showing that faulting postdates the 4.44 Ma volcanic eruption is seen in the flow direction of El Cerro Colorado (Fig. 8). The flows of El Cerro Colorado flowed to the southeast from a vent presently located in Guadalupita Valley and approximately 275 m below the remainder of the flow (O'Neill and Mehnert 1988).

We infer that offset of the Agua Fria flows in the northern part of the fault is due to faulting and, therefore, postdates flow emplacement. In contrast, O'Neill (1988) interpreted the northern part of this fault to have been active before the eruption of the Agua Fria flows. O'Neill (1988, p. B9) states

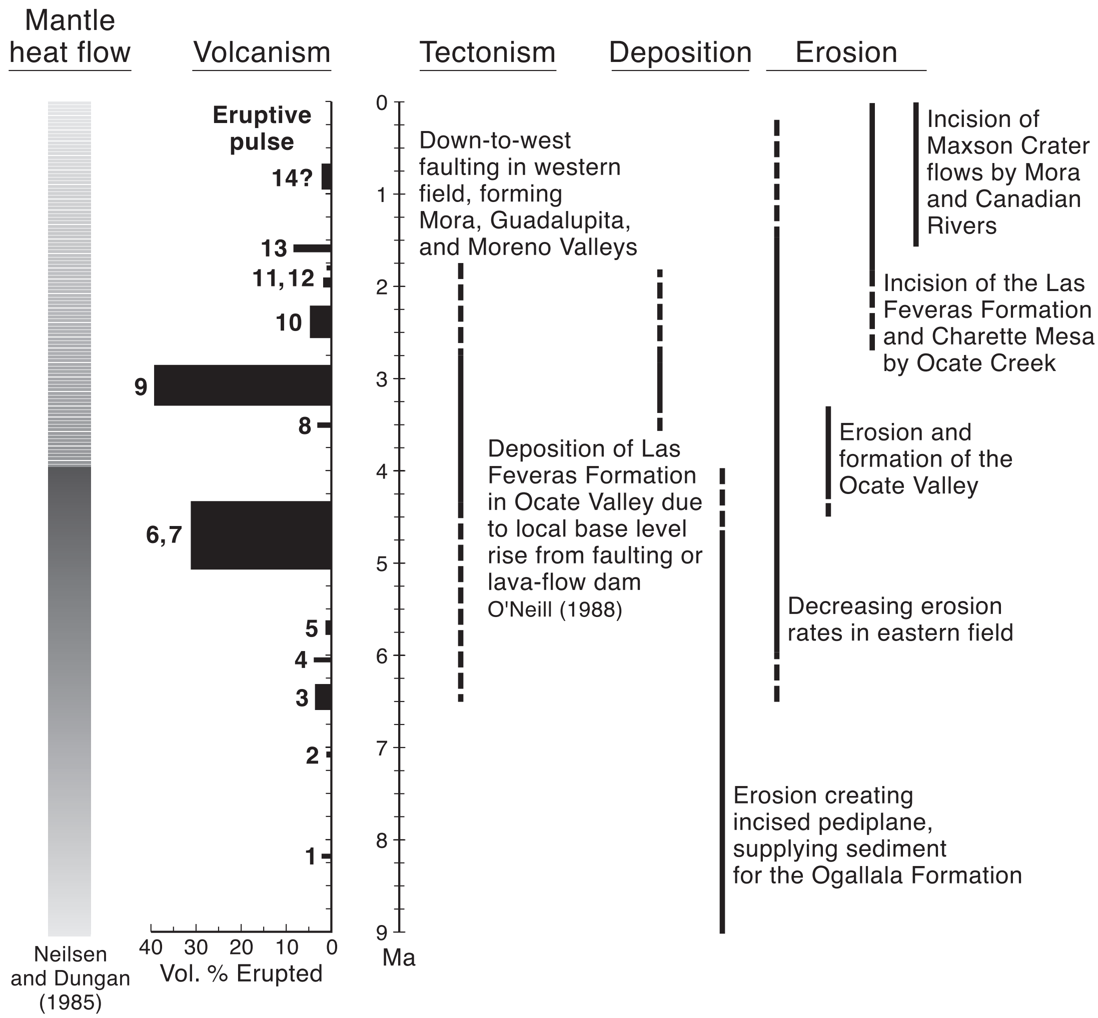

FIGURE 7—Timeline summarizing the geologic history of the Ocate volcanic field.

that the flows “appear to have cascaded over an arcuate west-facing scarp held up by steeply dipping Paleozoic sedimentary rocks that now separates the two levels.” Whether the north part of the fault was active before 4.48 Ma is not known. The southern part of the fault, however, could not have shown displacement before the eruption of the El Cerro Colorado flows at 4.44 Ma. We assume here that fault movement along the northern and southern parts was coeval.

Formation of the Ocate valley occurred after the 5.13–4.35 Ma eruptive episode, but before the eruption of Las Febres (mean of 4 samples: 3.01 ± 0.04 Ma) and the Cerro Pelon eruptions (OCA-012: 2.98 ± 0.03 Ma). Evidence for this is seen by the absence of 5.13–4.35 Ma lava flows and the presence of Las Febres and Cerro Pelon flows within the present-day valley (Fig. 5; O’Neill 1988). Formation of the fault-controlled half grabens of the Moreno, Mora, and Guadalupita valleys began after 4.35 Ma.

Evolution of the Ocate volcanic field

Figure 7 is a timeline of events constrained by the $^{40}Ar/^{39}Ar$ data that documents the volcanic and geomorphic history of the Ocate volcanic field. The history of the field began at ~8.2 Ma with the eruption of flows presently occupying Ocate Mesa and La Grulla Ridge. Until the widespread eruptions at 5.13–4.35 Ma, the field was marked by a period of small episodic eruptions throughout the field. Erosion of the field created a lower incised surface upon which the 5.13–4.35 Ma basalts were erupted, and supplied sediment for the Miocene Ogallala Formation (Frye and Leonard 1957, 1959; Scott 1975).

From 5.13 to 4.35 Ma a period of increased volcanism within the northern part of the field ensued with approximately 32 vol. % of the field being erupted during this time (28 km^3). A period of renewed uplift and faulting followed this major eruptive event. Down-to-the-west faulting was occurring within the western part of the field and led to the formation of the Moreno, Mora, and Guadalupita half-graben valleys. From 4.35–2.85 Ma the Ocate Valley was also forming by erosion.

After the 5.13–4.35 Ma eruptions, a hiatus in volcanic activity ensued until the eruption of White Peak in the Rivera Mesas area at 3.51 ± 0.03 Ma. A second major eruptive episode within the field followed, between 3.36–2.85 Ma when approximately 40 vol. % (36 km^3) of the field was erupted within the central part of the field. During this time deposition of the Las Feveras Formation within the Ocate Valley began.

After the 3.36–2.85 Ma eruptions a period of decreased eruptive activity ensued with small localized centers erupting within the central and southern parts of the field. Deposition of the Las Feveras Formation ceased and incision through it and Charette Mesa by Ocate Creek began and continues today. At 1.57 ± 0.04 Ma Maxson Crater erupted, producing approximately 8 vol. % (6.8 km^3) of the field. Flows emanating from Maxson Crater flowed southeasterly

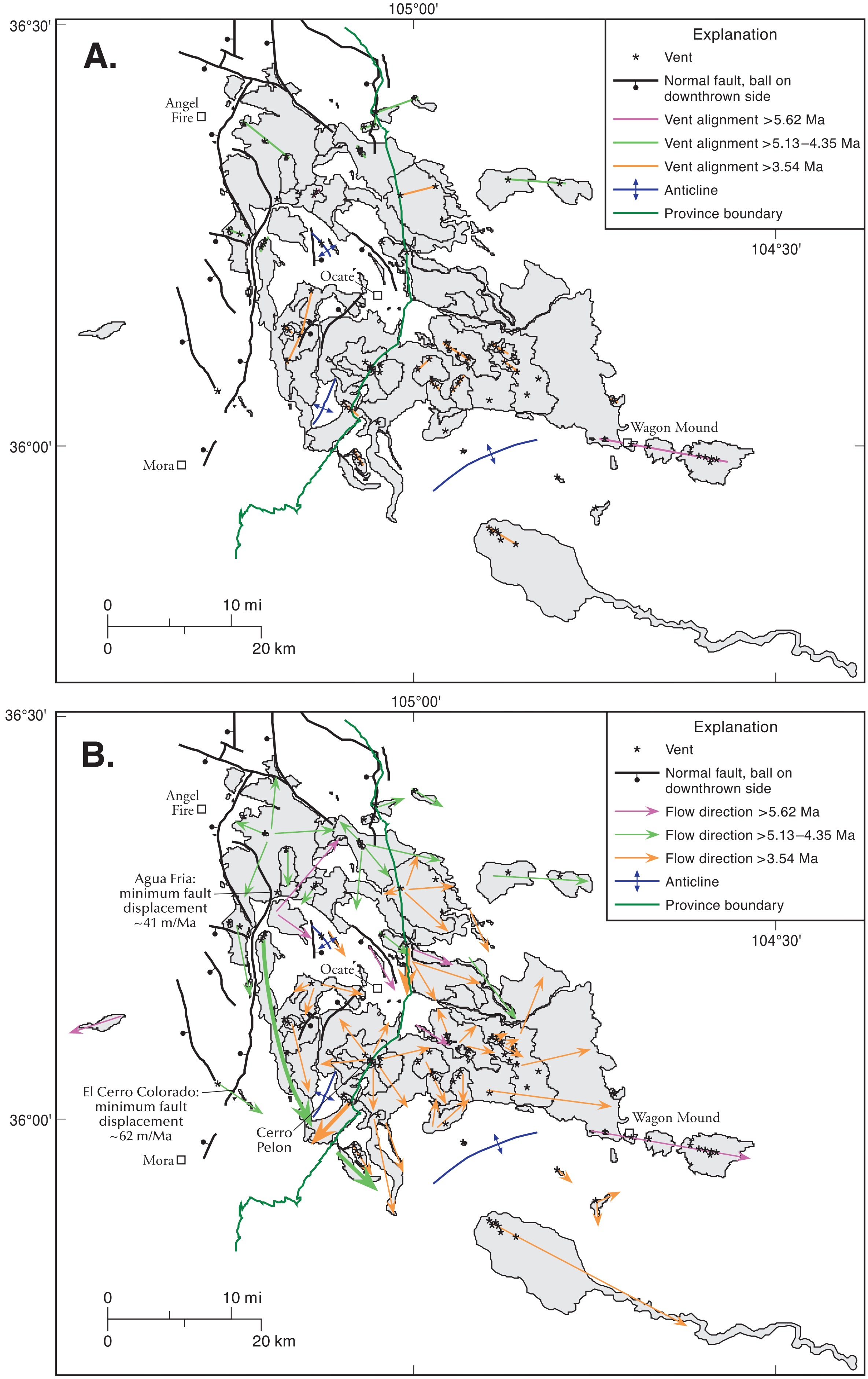
A.
36°30'
105°00'
Angel
Fire
Ocate
36°00'
Mora
Wagon Mound
104°30'
0
10 mi
0
20 km
Explanation
Vent
Normal fault, ball on downthrown side
Vent alignment >5.62 Ma
Vent alignment >5.13–4.35 Ma
Vent alignment >3.54 Ma
Anticline
Province boundary
B.
36°30'
105°00'
Angel
Fire
Agua Fria:
minimum fault
displacement
~41 m/Ma
Ocate
El Cerro Colorado:
minimum fault
displacement
~62 m/Ma
Cerro
Pelon
36°00'
Mora
Wagon Mound
104°30'
0
10 mi
0
20 km
Explanation
Vent
Normal fault, ball on downthrown side
Flow direction >5.62 Ma
Flow direction >5.13–4.35 Ma
Flow direction >3.54 Ma
Anticline
Province boundary

FIGURE 8—Source vents (**A**) and inferred flow directions (**B**) for Ocate volcanic field lavas. Arrows showing flow directions referred to in the text are enlarged.

into the canyon carved by the Mora River and continued for ~ 96 km before coming to a stop ~ 29 km past the Mora/Canadian confluence. The incision of the Maxson Crater flows by the Mora River began soon after and, at present, has eroded through the basalt and into the underlying sedimentary rocks.

Regional relationships

Figure 9 displays probability distribution diagrams for $^{40}Ar/^{39}Ar$ data from the Ocate and neighboring Raton–Clayton and Taos volcanic fields (Stroud 1997; Appelt 1998). All fields experienced eruptive activity near 5.7, 5.1, 4.7, 3.5, 3.0, and 2.3 Ma as well as an overall peak in eruptive activity from 5.1 to 2.3 Ma. The Ocate and Raton–Clayton fields share several nearly simultaneous eruptive episodes, and both show an overall episodic behavior, whereas the Taos field displays a more or less continuous eruptive behavior. The youngest eruption in the Taos and Ocate volcanic fields occurred ~1 Ma ago, whereas the youngest eruption in the Raton– Clayton field occurred ~50,000 yrs ago.

Conclusions

(1) The Ocate volcanic field formed episodically in approximately 16 eruptive volcanic pulses between 8.2 and 0.8 Ma. Volcanism generally progressed from north to south through this time period.

(2) Two volumetrically major eruptive episodes within the Ocate field, at 5.13–4.35 and 3.36–2.85 Ma, respectively produced 28 km3 and 40 km3 of lava, constituting 32% and 40% of the total eruptive volume of the field. The 5.13–4.35 Ma episode erupted from vents located in the northern part of the field, whereas the 3.36–2.85 Ma episode erupted from vents located in the central part of the field.

(3) After, and possibly soon before, the 5.13–4.35 Ma eruptions, onset of late Cenozoic down-to-the-west faulting began in the western part of the field.

(4) Minimum erosion rates calculated utilizing the inverted topography within the field appear to decrease from 6 Ma to present and correspond to the overall decrease in eruptive activity after the 5.13–4.35 and 3.36–2.85 Ma major volumetri-

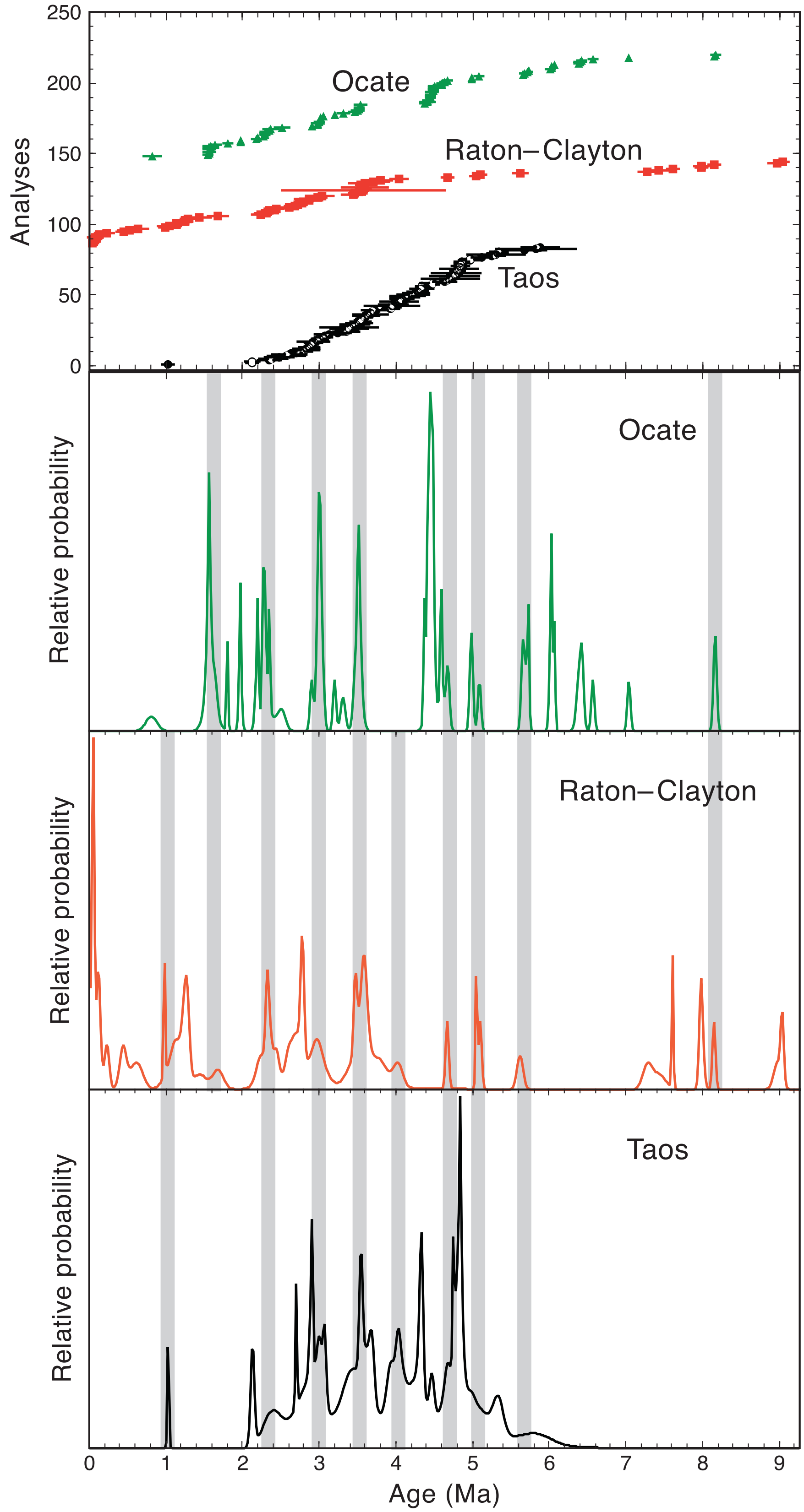

FIGURE 9–A comparison of the eruptive history of the Ocate field with the neighboring Taos and Raton–Clayton volcanic fields. The age-probability distribution curves are constructed by the method of Deino and Potts (1992). Shaded bars represent isochronous eruptive events shared by two or more fields.

cally eruptive episodes.

Acknowledgments

We would like to thank J. Michael O'Neill, Charles E. Chapin, and Matt Heizler for their helpful comments and reviews of the paper. We also thank Rich Esser, Lisa Peters, and Matt Heizler for their help with the $^{40}Ar/^{39}Ar$ analyses, and the landowners within the Ocate area for their permission to collect samples from their properties. Funding for this work was provided by the New Mexico Bureau of Geology and Mineral Resources.

References

Aldrich, M. J., Jr, Chapin, C. E., and Laughlin, A. W., 1986, Stress history and tectonic development of the Rio Grande rift, New Mexico: Journal of Geophysical Research, v. 91, no. B6, pp. 6199–6211.

Appelt, R. M., 1998, $^{40}Ar/^{39}Ar$ geochronology and volcanic evolution of the Taos Plateau volcanic field, northern New Mexico and southern Colorado: Unpublished M.S. thesis, New Mexico Institute of Mining and Technology, 149 pp.

Deino, A., and Potts, R., 1990, Single-crystal $^{40}Ar/^{39}Ar$ dating of the Olorgesailie Formation, Southern Kenya rift: Journal of Geophysical Research, v. 95, no. B. 6, pp. 8453–8470.

Frye, J. C., and Leonard, A. B., 1957, Ecological interpretations of Pliocene and Pleistocene stratigraphy in the Great Plains region: American Journal of Science, v. 255, no. 1, pp. 1–11.

Frye, J. C., and Leonard, A. B., 1959, Correlation of the Ogallala Formation (Neogene) in western Texas with the type localities in Nebraska: Bureau of Economic Geology, Texas University, Report of Investigations, no. 39, p. 116.

Lipman, P. W., Mehnert, H. H., and Naeser, C. W., 1986, Evolution of the Latir volcanic field, northern New Mexico, and its relation to the Rio Grande rift as indicated by K-Ar and fission-track dating: Journal of Geophysical Research, v. 91, pp. 7383–7402.

Mahon, K. I., 1996, The New "York" regression—application of an improved statistical method to geochemistry: International Geology Review, v. 38, pp. 293–303.

McDougall, I., and Harrison, T. M., 1999, Geochronology and thermochronology by the $^{40}Ar/^{39}Ar$ method, 2nd ed.: Oxford University Press, New York.

Nielson, R. L., and Dungan, M. A., 1985, The petrology and geochemistry of the Ocate volcanic field, north-central New Mexico: Geological Society of America, Bulletin, v. 96, pp. 296–312.

Olmsted, B. W., 2000, $^{40}Ar/^{39}Ar$ investigations of the Ocate volcanic field, north-central New Mexico: Unpublished M.S. thesis, New Mexico Institute of Mining and Technology, 86 pp.

O'Neill, J. M., 1988, Petrology and physiographic evolution of the Ocate volcanic field, north-central New Mexico, late Cenozoic physiographic evolution of the Ocate volcanic field: U.S. Geological Survey, Professional Paper 1478-B, pp.B1–B15.

O'Neill, J. M., and Mehnert, H. H., 1988, Petrology and physiographic evolution of the Ocate volcanic field, north-central New Mexico—the Ocate volcanic field- description of volcanic vents and the geochronology, petrology, and whole-rock chemistry of associated flows: U.S. Geological Survey, Professional Paper 1478-A, pp. A1–A30.

Pazzaglia, F. J., Duerker, K., and Wisniewski, P. A., 1999, Post-Laramide rock-uplift and exhumation of the Southern Rocky Mountains—evidence for the impact of "hot-mantle-blobs" (abs.): Geological Society of America, Abstracts with Programs, 31, no. 7, session 107, p. 245.

Samson, S. D., and Alexander, E. C., Jr., 1987, Calibration of the interlaboratory $^{40}Ar/^{39}Ar$ dating standard, Mmhb-1: Chemical Geology, v. 66, pp. 27–34.

Scott, G. R., 1975, Cenozoic surfaces and deposits in the Southern Rocky Mountains.: Geologic Society of America, Memoir 144, pp. 227–248.

Steiger, R. H., and Jäger, E., 1977, Subcommission on geochronology—convention on the use of decay constants in geo- and cosmochronology: Earth & Planetary Science Letters, v. 36, pp. 359–362.

Stroud, J. R., 1997, The geochronology of the Raton–Clayton volcanic field, with implications for the volcanic history and landscape evolution: Unpublished M.S. thesis, New Mexico Institute of Mining and Technology, 116 pp.